Main Manuscript for

Glycolytic enzymes form membrane-less condensates in the malaria parasite *Plasmodium falciparum* by sensing glucose levels

Ryuta Ishii[a], Takaya Sakura[b,c,*], Daniel Ken Inaoka[b,c,d], and Fuyuki Tokumasu[a,c,e,*]

[a]Department of Cellular Architecture Studies, Institute of Tropical Medicine (NEKKEN), Nagasaki University, Nagasaki 852-8523, Japan. [b]Department of Molecular Infection Dynamics, Institute of Tropical Medicine (NEKKEN), Nagasaki University, Nagasaki 852-8523, Japan. [c]School of Tropical Medicine and Global Health, Nagasaki University, Sakamoto, Nagasaki 852-8523, Japan. [d]Department of Biomedical Chemistry, Graduate School of Medicine, The University of Tokyo, Tokyo 113-0033, Japan. [e]Department of Laboratory Sciences, Gunma University Graduate School of Health Sciences, 3-39-22, Maebashi, Gunma, 371-8511, Japan.

[*]**Correspondence:** Takaya Sakura and Fuyuki Tokumasu

Email: takaya.sakura@nagasaki-u.ac.jp, ftokumasu@gunma-u.ac.jp

Author Contributions: R.I., T.S., D.K.I., and F.T. designed research; R.I., and T.S. performed research; R.I. analyzed data; and R.I., T.S., D.K.I., and F.T. wrote the paper.

Competing Interest Statement: The authors have no financial conflicts of interest to disclose concerning the study.

Classification: Biological Sciences, Cell Biology.

Keywords: Malaria parasite; Glycolytic enzymes; Liquid-liquid phase separation; Glycolytic bodies; Biomolecular condensates

This PDF file includes:

Main Text
Figures 1 to 6 and S1 to S4
Tables 1 and S1 to S3

Abstract

Recent studies have shown that liquid-liquid phase separation (LLPS) in cells can regulate essential cellular events, including metabolic processes. Glycolytic bodies (G-bodies) are biomolecular condensates formed through the LLPS of glycolytic enzymes, and they accelerate glycolysis to overcome hypoxic stress in several organisms. Although the asexual blood stage (ABS) of the human malaria parasite *Plasmodium falciparum* highly depends on glycolysis for energy production, there have been no reports of the formation of such G-bodies throughout the parasite's lifecycle. Using fluorescence tagging and live imaging, we found that G-body-like condensates containing phosphofructokinase 9 (PFK9) and phosphoglycerate kinase (PGK) were formed in the parasite cells after long-term culture under conditions of low glucose. These G-body-like structures appeared stable, but membrane staining and osmotic stress experiments suggested that the observed condensates were not associated with lipid membrane. Further microscopic observations and mathematical analyses of high signal-to-noise ratio images indicated that small condensates were formed transiently first, and these then gradually grew and stabilized in the cytosol. These results suggested that the formation of glycolytic enzyme condensates may be an important cellular response for adapting to blood sugar level oscillations in the host and maintaining the parasite's multiplication in the ABS.

Significance statement

Glycolytic bodies (G-bodies), which are biomolecular condensates formed through the liquid-liquid phase separation of glycolytic enzymes, can accelerate glycolysis to produce energy and overcome hypoxic stress. The parasites that cause malaria depend on glycolysis for energy production, but there have been no reports that these parasites form G-bodies. We demonstrated that membrane-less G-body-like structures formed in media containing low levels of glucose. Small condensates appeared first and over time, the condensates became larger and more stable. The formation of glycolytic enzyme condensates may be important for the malaria parasite to adapt to fluctuating blood sugar levels in the host. These results further our understanding of the cellular mechanisms for the survival of malaria parasites.

Main text

Introduction

Malaria is a devastating disease caused by *Plasmodium* parasites transmitted to humans from infected female *Anopheles* mosquitoes. After the asymptomatic liver stage, the parasite releases merozoites into the bloodstream to start the asexual blood stage (ABS), in which the number of parasites increases rapidly up to 10^{12} (1). During these rapid multiplications in the ABS, glycolysis is the parasites' primary source of energy production, given the fact that several tricarboxylic acid cycle enzymes and the β subunit of adenosine triphosphate (ATP) synthase are dispensable (2-4). Although glycolysis is essential for the blood stage of the parasite, the reaction rates for the glycolysis steps change drastically during intraerythrocytic development (5), which may be difficult to explain by the simple regulation of enzyme expression levels, considering the results of transcriptome analysis (6, 7).

To control the activity of sequential multi-enzyme reactions, cells utilize liquid-liquid phase separation (LLPS) to condense enzymes, substrates, and products within a droplet, which usually allows stable control of the process. For example, purine biosynthesis-related enzymes are compartmentalized in clusters called purinosomes in human cells under purine-depleted conditions to accelerate enzyme reactions (8, 9). Purinosomes contain at least ten enzymes in the purine biosynthesis and salvage pathways, and these enzymes efficiently convert phosphoribosyl pyrophosphate to adenosine monophosphate and guanosine monophosphate (10). Another example of LLPS-induced enzyme reaction activation is the "G-body," which is formed under hypoxia by the condensation of glycolytic enzymes. The assembly of glycolytic enzymes in response to hypoxia was first observed in 2011, when glyceraldehyde-3-phosphate dehydrogenase

(GAPDH), the glycolytic enzyme catalyzing the sixth step of glycolysis, was observed to form foci in HeLa cells under hypoxia (11). Subsequently, Miura et al. reported that several glycolytic enzymes were condensed in foci in *Saccharomyces cerevisiae* under hypoxia (12). The yeast Pfk2 has a 'disordered region' that lacks a rigid three-dimensional structure. Deletion of this region resulted in failure of the G-body formation, suggesting that Pfk2 served as one of the scaffold proteins of G-bodies, and the disordered region drove the condensation of glycolytic enzymes (13). The detailed components of the G-bodies were identified by isolation and proteome analysis of G-bodies from yeast cells (14). G-bodies contain not only glycolytic enzymes but also chaperones, proteasomal subunits, and fatty acid synthesis-related proteins, suggesting that G-body formation is closely linked with other metabolic pathways and ATP-dependent cellular processes. Glycolysis has been shown to be accelerated by G-body formation to produce more ATP, which is required to increase cell survival (14). Local high concentrations of PFK-1.1, the *Caenorhabditis elegans* ortholog of PFK, were also reported to trigger G-body formation. PFK-1.1 was distributed unevenly in neurons, but helped to satisfy the local energy demands in normoxia (15). G-bodies were thought to be required to narrow down the target area and sustain synaptic function under stress.
To take advantage of glycolytic enzyme condensation, kinetoplastids and diplonemids, such as *Trypanosoma cruzi*, a protozoan parasite causing Chagas disease, have a membrane-bound organelle called a glycosome (16). This structure contains most of the glycolytic enzymes of these protists and may have characteristics similar to those of G-bodies. However, there have not been any reports on membrane-bound or membrane-less glycolytic organelle formation in *Apicomplexan* parasites, including *Plasmodium falciparum* (*Pf)*, although *Pf* highly depends on glycolysis as an energy source.
We hypothesized that G-bodies are also formed in the cells of *Pf* parasites and may play a critical role in metabolic regulation. Several of the glycolytic enzymes of *Pf* are disordered proteins, and *Pf*PFK9, the ortholog of yeast Pfk2, has one or more disordered regions, which implies that *Pf*PFK9 may contribute to G-body formation in the parasite cells. In the present study, PFK9 formed transient and stable condensates in the parasite cells, and they were enzyme-specific and also membrane-less structures. In addition, mathematical analyses indicated that small PFK9 condensates were formed in 6 h, which may be essential for the parasite to adapt to changes in glucose levels in the human body.

Results

PFK9 condensates appeared in *Pf* parasites under low-glucose conditions.

To visualize the formation of G-body-like structures in the parasite cells, we generated transgenic parasites that expressed fluorescently tagged PFK9 at the *C*-terminus. The *C*-terminus was selected because tagging of the disordered *N*-terminal sequence may affect the LLPS of PFK9 (Fig. 1A). We used a pKIC-ter plasmid for inducing selection-linked integration (SLI) (17). SLI allows the expression of a target protein to be controlled by an endogenous promoter, which is important for LLPS studies, as slight modifications of the expression level of target proteins easily influence LLPS. The plasmid had a homologous PFK9 *C*-terminal sequence followed by mNeonGreen (mNG) (18), 2xMyc tag, a tandem sequence of P2A and T2A skip peptides (19), and bacterial neomycin-kanamycin phosphotransferase II (NPTII) as a selection marker. Skip peptides allow the physically separated expression of a tagged target protein and NPTII (Fig. 1B). Diagnostic PCR suggested the successful insertion of the plasmid sequence into the parasite genome (Fig. 1C). The expression of tagged PFK9 was also confirmed by western blotting (Fig. 1D); however, no G-body-like structures were observed in the live imaging (Fig. 1E), unlike a previous report that showed that PFK9 droplet-like structures were formed in the trophozoite state using immunofluorescence assay (20). Therefore, several stimulation methods to facilitate G-body formation were investigated, including heat shock, culture at high parasitemia, and treatment with respiratory chain inhibitors, but none of these conditions could induce the formation of G-body-like structures. PFK9 condensates were only observed when the parasites were cultured for more than 72 h in a medium with 5 mM glucose (≈half the glucose concentration of Roswell Park Memorial Institute media

(RPMI)) (Fig. 2A and 2B), corresponding to a fasting blood glucose concentration. The clustering percentage, which represents the fraction of pixels with a normalized intensity below a given threshold (21), increased to 123% when the parasite was cultured in a 5 mM low glucose medium (Fig. 2C). Interestingly, there was no difference in transcriptome and metabolome between standard and low-glucose cultured parasites (Fig. S1 and S2). Glucose concentrations less than 5 mM led to early cell death, possibly because of the malfunction of host erythrocytes, and we did not observe any additional PFK9 condensates. These observations suggested that PFK9 condensates were formed through slight but continuous low glucose stress, not acute glucose decreases that do not occur in the human body.

PFK9 condensates behave like membrane-less structures.

Large PFK9 condensates were quite stable and did not fuse with other condensates for at least 30 min (Fig. 3A). The physical properties of PFK9 condensates in parasite cells were examined by fluorescence recovery after photobleaching (FRAP) analysis. However, the small size of condensates with respect to the limited laser spot size did not allow to collect fluorescence signals specifically from condensates because PFK9 signals outside the condensates obscured the signal origins.

To investigate whether the PFK9 condensates were membranous structures, parasitized erythrocytes were stained with Di-4-ANEPPDHQ, a dye that shows fluorescence only when in a phospholipid membrane (22). The G-body-like condensates were devoid of the Di-4-ANEPPDHQ signal, whereas the parasite membranes showed fluorescence, indicating that the G-body-like condensates were membrane-less organizations formed through LLPS (Fig. 3B).

For further characterization of the PFK9 condensates, hyperosmotic experiments were performed to study condensate formation with temporal changes in cellular protein concentrations. Recent studies have shown that hyperosmotic stress can cause LLPS of several proteins because osmotic pressure compresses the cell volume and increases the protein concentration and macromolecular crowding (23). In addition, the local concentration of PFK was likely the key determinant of G-body formation in *C. elegans* (24). After the induction of hyperosmotic stress by the addition of 50 mM of sodium chloride, the rapid formation of PFK9 condensates was observed within 5 min (Fig. 3C and 3D). Furthermore, unlike the stable PFK9 condensates formed through long-term low glucose culture, these structures dissolved immediately after the hyperosmotic stress was removed. These observations suggested that an increase in the local PFK9 concentration and macromolecular crowding could induce the formation of PFK9 condensates in the parasite.

Total internal reflection fluorescence (TIRF) imaging indicates early formation of small PFK9 condensates.

Although we could successfully observe PFK9 condensates in low-glucose cultures, the formation of these condensates did not always occur under fixed conditions, possibly because of differences in the conditions of the host cells caused by the daily maintenance of the cell cultures. In addition, the PFK9 condensates were quite stable, and the formation was irreversible under isotonic conditions, indicating that these condensates had more rigid physical properties compared with the common G-bodies in other organisms. It has been demonstrated that G-bodies become more rigid over time (24), but no growing or maturing PFK9 condensates were observed in the parasite. Considering the high expression levels of PFK9 throughout the ABS of the parasite, the fluorescence of PFK9-mNG from outside the focal plane gave indistinct images even when we used confocal microscopy. To obtain images with a higher signal-to-noise ratio, TIRF imaging was performed for the parasites that showed no clear PFK9 condensate formation after a 72 h low

glucose culture. TIRF imaging could be used to detect the fluorescence of PFK9-mNG present within ≈120 nm from the coverslip in our setting. The distribution of PFK9 changed with changing glucose concentrations, and uneven signals were evident, especially under low glucose conditions (Fig. 4A). Power spectrum analysis of the fluorescence intensity profile (25) showed that parasites cultured under low glucose conditions showed a steeper slope in the power plot because of the higher power values at lower frequencies, which indicated the existence of larger PFK9 clusters (Fig. 4B). The time-dependent power spectra analysis also suggested the existence of larger PFK9 clusters after at least 6 h of low glucose culture (Fig. 4C). To elucidate the size of the PFK9 clusters, we applied autocorrelation analysis to the TIRF images. Hwang et al. demonstrated that two-dimensional spatial autocorrelation analysis can be used to deduce the size of protein domains (26), and we expanded this approach to estimate the average protein cluster size of *Pf*-infected erythrocytes (25). For the angle-averaged autocorrelation, the functions for both standard-cultured and low glucose-cultured parasites could be fitted to a single-peak Gaussian curve, and the cluster sizes were estimated from the full width at half max (FWHM) value (Fig.4D and Table 1). These results implied that larger PFK9 clusters existed in parasites cultured under low glucose conditions, even though the estimated sizes were bigger than we expected, possibly because of the pixel size of the images (100 nm/pixel).

Phosphoglycerate kinase (PGK) also forms condensates under low glucose conditions.

To investigate whether the condensate formation also occurred for other glycolytic enzymes, several transgenic parasites expressing mNG-tagged glycolytic enzymes were generated using SLI. Of the nine glycolytic enzymes, except PFK9, six enzymes were successfully tagged and had the expression of the tagged proteins confirmed (Fig. S3). However, the tagging of fructose-bisphosphate aldolase (FBPA; PF3D7_1444800), GAPDH (PF3D7_1462800), and enolase (ENO; PF3D7_1015900) was not successful, possibly because of the toxic effects of the *C*-terminus tagging of these genes and further investigation is needed. The obtained transgenic parasites were cultured under low glucose conditions for 80 h, and only PGK (PF3D7_0922500) formed similar condensates to that of PFK9 in the cytosol (Fig. 5). These results suggested the possibility that multi-enzymatic G-body-like structures may be formed under low glucose conditions to overcome the low glucose stress via the acceleration of glycolysis. In addition, the results indicated that these structures were formed by specific enzymes in the parasites rather than by the stress-induced non-specific aggregation of the cytosol.

Discussion

In the present study, PFK9 was the primary enzyme investigated because 1) glycolysis is one of the most important processes in the *Pf* lifecycle; 2) PFK9 is the most investigated protein of the G-body components; and 3) *Pf*PFK9 also has disordered regions, which are required for G-body formation in yeast. It was unexpected that PFK9 did not form condensates in a steady state, probably because the parasite was already in a hypoxic condition (27), and the function of G-bodies in *Pf* may differ from that in other organisms. In addition, it should be noted that RPMI 1640-based standard culture medium provides for a higher growth rate than human serum because of the supraphysiological nutrient levels in RPMI (28, 29), and the metabolic conditions in cultured parasites and the need for G-bodies might differ from that of the parasite in vivo. This perspective led to the successful observation of G-body-like structures under fasting blood sugar-level conditions.

The long-term low glucose culture results for the seven parasites that expressed tagged glycolytic enzymes suggested that PFK9 and PGK were the components of the G-body-like structures. In the present study, *C*-terminal-tagged FBPA, GAPDH, and ENO-expressing parasites were not obtained successfully. The crystal structure analyses of FBPA and GAPDH have suggested that the working units are a homodimer and a homotetramer, respectively (30, 31). The results of recombinant *Pf*ENO purification also indicated that a homodimer was formed (32); therefore, the

C-terminal tagging of these proteins may have disrupted the multimer formation and resulted in the cell death of the parasite. Crystal structure analysis of PGK demonstrated that it did not have a disordered region (33), suggesting that PFK9 may be the scaffold of the G-body-like structures. Consistent with this proposal, the purified disordered regions of PFK9 with and without a GFP tag aggregated even at low concentrations (< 2 μM), suggesting strong intermolecular or intramolecular interactions of the PFK9 protein occurred in these regions (Fig. S4). From a functional aspect, PFK9 and PGK both utilize ATP and ADP. Because ATP can act as a hydrotrope in cells (34), PFK9 and PGK interactions and the formation of G-body-like structures may be regulated by the ATP levels in the parasite cells, which could be reasonable as a feedback process of the primary ATP source.

The results for membrane staining and osmotic stress conditions suggested that the condensation of PFK9 was membrane-less. Interestingly, unlike condensates formed after long-term low glucose culture, the formation of osmotic stress-induced PFK9 condensates was reversible. This result indicated that the formation of G-body-like structures in cells is initially reversible, and reaching the critical local concentration induces the irreversible formation of condensates, probably due to the strong intramolecular interaction force. Because LLPS is essentially dependent on the concentration of a scaffold protein, the existence of a critical local concentration strongly supports the idea that the condensates were formed through the LLPS of PFK9 (35). The exact mechanism for triggering condensate formation was not identified in the present study. However, considering that the PFK9 expression level did not change even after low glucose culture (Fig. S1), there is likely to be some machinery for increasing the local PFK9 interactions and concentrations, such as post-translational modifications or an increase in other cluster-facilitating proteins (Fig. 6A). Another possibility for a PFK9-condensation facilitator is a non-protein scaffold molecule, such as RNA. It has been reported that long noncoding RNA could assemble a metabolon of several glycolytic enzymes to overcome metabolic stress (36), and a similar phenomenon may occur in the parasite cytosol. Fusing an RNase to the *C*-terminus of PFK9 may be able to determine the role of RNA in condensate formation, as has been performed in yeast (37). A limitation of the present study was the lack of direct observations of liquid-like behaviors in PFK9 condensates because of technical difficulties with the FRAP analysis and the difficulty of observing the fusion of PFK9 condensates in small parasite bodies. Further investigations are required to investigate the LLPS of PFK9 using other methods, such as observations using fluorescence correlation spectroscopy, which detects changes in molecular diffusion when condensates fuse with each other and become larger clusters (38).

Although the existence of small reversible PFK9 condensates was hypothesized, we were unable to observe these structures using standard microscopy. TIRF imaging provided images with a heterogeneous distribution of PFK9 even when the large condensates were not visible using conventional confocal microscopy, and TIRF imaging also showed the fast movement of PFK9 within the parasite cytosol. The fast mixing of the PFK9 condensates may be one of the reasons why conventional confocal microscopy showed homogeneous PFK9 distribution because the slow scanning speed and image averaging resulted in the acquisition time being longer than 10 s. Because confocal and epi-fluorescence microscopy has limitations in the optical resolution, structures less than 300–500 nm in diameter cannot be distinguished, and autocorrelation analysis was used to identify the existence of PFK9 condensates in the parasite after low glucose culture. Time-course TIRF analysis of parasites cultured under low glucose conditions suggested that small condensates were formed within 6 h. Considering that 5 mM glucose corresponds to a fasting blood sugar level, this result indicated that parasites utilize G-body-like structures for adapting to blood sugar level oscillations in the human body (Fig. 6B). The activity of the primary energy source may be finely regulated by the LLPS of glycolytic enzymes to adjust to the nutritional condition of the host, which may differ appreciably after an increase in the parasite load (39).

More studies will be needed to clarify the significance and nature of PFK9 condensation by measuring the growth rates and glycolytic activity of the parasite under physiological conditions. However, given the fact that the metabolite levels of glycolysis did not change even after long-term low glucose stress (Fig. S2 and Table S4), PFK9 condensation is likely to be important for maintaining glycolysis activity under conditions of low substrate levels.

In summary, we found that PFK9 and PGK form G-body-like membrane-less condensates in low glucose conditions. These condensates became larger and more rigid after long-term low glucose culture, but mathematical analysis suggested that small condensates were formed in the short term, possibly explaining the mechanism of the parasite's adaptation to the changes in human blood glucose levels.

Materials and methods

Culture of *Pf* parasite

Pf 3D7 parasites (40) were maintained in complete medium [CM; RPMI 1640 medium with 25 mM HEPES, supplemented with 25 mg/L gentamicin, 50 mg/L hypoxanthine, 23.8 mM sodium bicarbonate, and 0.5% Albumax II at 2% hematocrit of O+ human erythrocytes at 37 °C with a mixed gas (5% O_2, 5% CO_2, and 90% N_2)]. The parasite culture was diluted every 2 or 3 days to maintain the parasitemia between 0.1% and 5%, typically.

Plasmid construction

For the fluorescent tagging of glycolytic enzymes, SLI was induced by transfection of a pKIC-ter plasmid derived from a pD3 plasmid (41, 42), which has human dihydrofolate reductase and NPTII as selection markers against WR99210 and G418, respectively. Myc tag, a green fluorescent protein mNG tag, and a skip peptide P2A and T2A tandem sequence were synthesized and cloned into pD3 by a seamless ligation cloning extract (SLiCE) reaction (43), resulting in the plasmid pKIC-ter. The pKIC-ter plasmid was restricted with NotI, and the *C*-terminal sequence of the gene of interest amplified from the 3D7 genomic DNA (gDNA) or synthesized DNA (Table S1) was inserted using SLiCE. The primers used for the amplification are summarized in Table S2.

Transfection and drug selection of *Pf*

Erythrocytes were suspended in cytomix (44) [120 mM KCl, 0.15 mM $CaCl_2$, 10 mM K_2HPO_4/KH_2PO_4 (pH 7.6), 25 mM HEPES-KOH (pH 7.6), 2 mM ethylene glycol tetraacetic acid (pH 7.6), and 5 mM $MgCl_2$, adjusted to pH 7.6 with KOH], centrifuged, and the supernatant was removed. Fifty micrograms of plasmid DNA and 150 µL of packed erythrocytes were mixed, and the volume was made up to 400 µL with cytomix in a 0.2 cm electroporation cuvette. Electroporation was performed with GenePulser (Bio-Rad Laboratories, Hercules, CA, USA) using the conditions: voltage = 310 V; capacitance = 975 µF; resistance = ∞; and cuvette = 2 mm. Erythrocytes were washed with cold RPMI twice and then suspended in CM. The 3D7 parasite was inoculated to the electroporated erythrocytes at 0.1%–0.3% parasitemia and cultured in a flask as described above. When parasitemia reached ≈5%, drug selection was initiated by adding final 1 nM WR99210 to the culture, and culturing was continued for 10 days. After the parasite re-emergence, 400 µg/mL G418 was added to the culture for 10 days to select the parasite with genome insertion of the plasmid sequence.

Diagnostic PCR

The gDNA of the parasite was purified with DNeasy Blood & Tissue kits (QIAGEN, Hilden, Germany). Insertion of the plasmid sequences was confirmed by PCR using gDNA as templates. Primers p1 to p4 (Table S2) were used for genotyping.

Western blotting

The parasite culture was pelleted and suspended in PBS containing 1 × complete protease inhibitor cocktail (Roche, Basel, Switzerland). Saponin (at a final concentration of 0.15%) was added to the solution and incubated on ice for 8 min. The parasite was pelleted by centrifugation at 16,900 × *g* and washed twice with PBS containing 1 × complete protease inhibitor cocktail. NuPAGE LDS sample buffer containing NuPAGE sample reducing agent (Invitrogen, Waltham, MA, USA) was added to the pellet to obtain 10^6 parasites/µL and heated at 70 °C for 10 min. A sample of the

prepared solution (10 to 25 µL) was applied to a NuPAGE 4% to 12% Bis-Tris mini protein gradient gel, and SDS-PAGE was performed in MOPS SDS running buffer at 200 V for 40 min. Membrane transfer to the polyvinylidene difluoride membrane was performed using the XCell II blot module and NuPAGE transfer buffer at 30 V for 1 h. The membrane blocking was performed with Bullet Blocking One (Nacalai, Kyoto, Japan) for 5 min at room temperature. PBS containing 5% Bullet Blocking One was used for antibody dilution. The antibodies and reaction conditions used in the present study are summarized in Table S3. SuperSignal West Pico PLUS chemiluminescent substrate (Invitrogen) was used to generate chemiluminescent signals, and images were taken using a Luminograph II (Atto, Tokyo, Japan) or FUSION-FX6.EDGE (Vilber, Collégien, France).

G-body induction

Low glucose CM [glucose-free RPMI 1640 (Thermo Fisher Scientific, Waltham, MA, USA) medium supplemented with 25 mg/L gentamicin, 50 mg/L hypoxanthine, 25 mM HEPES, 23.8 mM sodium bicarbonate, 0.5% Albumax II, and 5 mM glucose] was used for the induction of G-body formation. The parasite cultured in the same CM but supplemented with 10 mM glucose was used as a negative control. The 3D7 parasite expressing mNG-tagged glycolytic enzymes was diluted in 2% hematocrit low glucose CM at 0.1%–0.3% parasitemia and maintained for 3 to 4 days until G-bodies were observed by microscopy.

Live imaging of the parasite

Hoechst 33258 was added to the parasite culture at 2 µg/mL for nuclear staining. After 30 min of incubation at 37 °C, the parasite culture was washed with CM, centrifuged, applied on a microscope slide, and sealed with a coverslip. Images were taken by a LSM780 (Zeiss, Oberkochen, Germany) or DMi8 (Leica, Wetzlar, Germany) camera.

Calculation of clustering percentage

The image analyses were performed using ImageJ Fiji (45). For calculating the clustering percentage (21), parasite cell images were automatically cropped after performing ‘subtract background,’ thresholding using Huang's fuzzy thresholding method, running ‘analyze particle’ and ‘enhance contrast.’ The clustering percentage was calculated from the areas measured after thresholding at an intensity of 90 divided by the areas measured without thresholding. Graphs were prepared using GraphPad Prism (GraphPad Software, La Jolla, MA, USA), and statistical analyses were performed with EZR (Saitama Medical Center, Jichi Medical University, Saitama, Japan) (46).

Lipid membrane staining

The PFK9-mNG expressing parasite was cultured in 10 or 5 mM glucose-containing CM for 4 days. The parasite was centrifuged, and the supernatant was replaced with 5 mM glucose-containing RPMI 1640 with Di-4-ANEPPDHQ (Thermo Fisher Scientific) at 2 µg/mL, and the mixture was incubated at 37 °C for 30 min. The parasite was washed with 10 or 5 mM glucose-containing CM, centrifuged again, applied on a microscope slide, and sealed with a coverslip. Images were taken using an LSM780 microscope.

Osmotic stress induction

The PFK9-mNG expressing parasite cultured in the standard CM was centrifuged and suspended in a medium containing 50 or 100 mM sodium chloride. After 5 min of incubation at 37 °C, the parasite was centrifuged, applied on a microscope slide, and sealed with a coverslip. Images were taken using a LSM780 microscope. Graphs were prepared using GraphPad Prism, and statistical analyses were performed with EZR.

TIRF imaging

The PFK9-mNG-expressing parasite was cultured in 10 or 5 mM glucose-containing CM for 72 h and purified by magnetic separation. The parasite cells were applied on coverslips coated with poly-D-lysine (4–15 kDa) at 10 µg/cm^2 and incubated at 37 °C for 20 min, then the coverslips were

washed with PBS twice. Five microliters of spent medium was applied on a microscope slide and sealed with the coverslip. Images were taken using a LSM780 microscope.

Power spectrum and autocorrelation analyses of TIRF images

Image analysis was performed with ImageJ Fiji and OriginPro 2023b (Lightstone, Park Avenue, NY, USA). For power spectrum analysis, background subtraction was performed and at least three segmented lines in the parasite cytosol longer than 5 µm were drawn and the intensity was measured along these lines using Fiji. The 8-bit intensity data with distance were transferred to OriginPro, and a fast Fourier transform (FFT) was performed to obtain the power spectrum. The power spectrum was normalized by the highest value, then plotted on a double logarithmic scale, and linear regression analysis was performed with OriginPro. The 25 × 25 pixel intensity of the parasite cytosol was exported for autocorrelation analysis using Fiji. The data were transferred to OriginPro, and a two-dimensional FFT was performed to obtain the power, followed by a two-dimensional inverse FFT to obtain the real number matrix, corresponding to the two-dimensional spatial autocorrelation function (26). The autocorrelation function was normalized over all angles and fitted with a single Gaussian function with OriginPro. PFK9 cluster sizes were estimated from the FWHM value of the fitting.

Metabolome analysis

The PFK9-mNG expressing parasite was purified by magnetic separation using a MACS separator with LS columns (Miltenyi Biotech, Bergisch Gladbach, Germany) and inoculated to CM containing erythrocytes at 2.5% hematocrit. After 6 h of incubation at 37 °C, sorbitol synchronization was performed to obtain the ring stage parasites (6 h synchronization window), which were suspended in 10 or 5 mM glucose-containing CM, and incubated at 37 °C for 78–80 h. The parasite was purified by magnetic separation, centrifuged, and suspended in methanol, followed by freezing in liquid nitrogen. The quantification of 116 metabolites and statistical analysis was performed by Human Metabolome Technologies.

Transcriptome analysis

The PFK9-mNG expressing parasite was purified by magnetic separation and inoculated to CM containing erythrocytes at 2.5% hematocrit. After 3 h of incubation at 37 °C, sorbitol synchronization was performed to obtain the ring stage parasites (3 h synchronization window), which were suspended in 10 or 5 mM glucose-containing CM, and incubated at 37 °C for 24 or 36 h. The total RNA was purified with a PureLink RNA Mini kit (Thermo Fisher Scientific) and sent to Novogene for reverse transcription, sequencing, mapping to the *Pf* 3D7 genome, and statistical analysis. The data have been deposited with links to BioProject accession number PRJDB17842 in the DDBJ BioProject database (https://www.ddbj.nig.ac.jp/bioproject/).

Acknowledgments and funding sources.

This work was supported by JSPS KAKENHI Grant Number JP22K07045. This work was also partially funded by the Nagasaki University WISE Programme. We thank Eizo Takashima for providing anti-EXP2 antibody. The Japanese Red Cross Society provided human erythrocytes. This study was conducted (in part) at the Joint Usage / Research Center on Tropical Disease, Institute of Tropical Diseases, Nagasaki University, Japan. Victoria Muir, PhD, from Edanz (https://jp.edanz.com/ac) edited a draft of this manuscript.

References

1. M. Duffey *et al.*, Assessing risks of *Plasmodium falciparum* resistance to select next-generation antimalarials. *Trends in Parasitology* **37**, 709-721 (2021).
2. J. E. Salcedo-Sora, E. Caamano-Gutierrez, S. A. Ward, G. A. Biagini, The proliferating cell hypothesis: a metabolic framework for Plasmodium growth and development. *Trends Parasitol* **30**, 170-175 (2014).
3. F. Evers *et al.*, Composition and stage dynamics of mitochondrial complexes in *Plasmodium falciparum*. *Nature Communications* **12**, 3820 (2021).
4. A. Sturm, V. Mollard, A. Cozijnsen, C. D. Goodman, G. I. McFadden, Mitochondrial ATP synthase is dispensable in blood-stage *Plasmodium berghei* rodent malaria but essential in the mosquito phase. *Proc Natl Acad Sci U S A* **112**, 10216-10223 (2015).
5. R. Shivapurkar *et al.*, Evaluating antimalarial efficacy by tracking glycolysis in *Plasmodium falciparum* using NMR spectroscopy. *Sci Rep* **8**, 18076 (2018).
6. L. Chappell *et al.*, Refining the transcriptome of the human malaria parasite *Plasmodium falciparum* using amplification-free RNA-seq. *BMC Genomics* **21**, 395 (2020).
7. M. Kucharski *et al.*, A comprehensive RNA handling and transcriptomics guide for high-throughput processing of Plasmodium blood-stage samples. *Malar J* **19**, 363 (2020).
8. S. An, R. Kumar, E. D. Sheets, S. J. Benkovic, Reversible Compartmentalization of *de Novo* Purine Biosynthetic Complexes in Living Cells. *Science* **320**, 103-106 (2008).
9. H. Zhao *et al.*, Quantitative analysis of purine nucleotides indicates that purinosomes increase *de novo* purine biosynthesis. *J Biol Chem* **290**, 6705-6713 (2015).
10. A. M. Pedley, V. Pareek, S. J. Benkovic, The Purinosome: A Case Study for a Mammalian Metabolon. *Annu Rev Biochem* **91**, 89-106 (2022).
11. T. A. Agbor *et al.*, Small ubiquitin-related modifier (SUMO)-1 promotes glycolysis in hypoxia. *J Biol Chem* **286**, 4718-4726 (2011).
12. N. Miura *et al.*, Spatial reorganization of *Saccharomyces cerevisiae* enolase to alter carbon metabolism under hypoxia. *Eukaryot Cell* **12**, 1106-1119 (2013).
13. G. G. Fuller *et al.*, RNA promotes phase separation of glycolysis enzymes into yeast G bodies in hypoxia. *eLife* **9**, e48480 (2020).
14. M. Jin *et al.*, Glycolytic Enzymes Coalesce in G Bodies under Hypoxic Stress. *Cell Rep* **20**, 895-908 (2017).
15. S. Jang *et al.*, Glycolytic Enzymes Localize to Synapses under Energy Stress to Support Synaptic Function. *Neuron* **90**, 278-291 (2016).
16. W. Quiñones *et al.*, Structure, Properties, and Function of Glycosomes in *Trypanosoma cruzi*. *Frontiers in Cellular and Infection Microbiology* **10** (2020).
17. T. Spielmann *et al.*, Selection linked integration (SLI) for endogenous gene tagging and knock sideways in *Plasmodium falciparum* parasites. *Protocol Exchange* 10.1038/protex.2017.022 (2017).
18. N. C. Shaner *et al.*, A bright monomeric green fluorescent protein derived from *Branchiostoma lanceolatum*. *Nature Methods* **10**, 407-409 (2013).
19. Z. Liu *et al.*, Systematic comparison of 2A peptides for cloning multi-genes in a polycistronic vector. *Sci Rep* **7**, 2193 (2017).
20. B. M. Mony, M. Mehta, G. K. Jarori, S. Sharma, Plant-like phosphofructokinase from *Plasmodium falciparum* belongs to a novel class of ATP-dependent enzymes. *International Journal for Parasitology* **39**, 1441-1453 (2009).
21. A.-M. Ladouceur *et al.*, Clusters of bacterial RNA polymerase are biomolecular condensates that assemble through liquid–liquid phase separation. *Proceedings of the National Academy of Sciences* **117**, 18540-18549 (2020).

22. L. Jin, A. C. Millard, J. P. Wuskell, H. A. Clark, L. M. Loew, Cholesterol-enriched lipid domains can be visualized by di-4-ANEPPDHQ with linear and nonlinear optics. *Biophys J* **89**, L04-06 (2005).
23. A. P. Jalihal *et al.*, Hyperosmotic phase separation: Condensates beyond inclusions, granules and organelles. *Journal of Biological Chemistry* **296** (2021).
24. S. Jang *et al.*, Phosphofructokinase relocalizes into subcellular compartments with liquid-like properties *in vivo*. *Biophys J* **120**, 1170-1186 (2021).
25. F. Tokumasu *et al.*, Band 3 modifications in *Plasmodium falciparum*-infected AA and CC erythrocytes assayed by autocorrelation analysis using quantum dots. *Journal of Cell Science* **118**, 1091-1098 (2005).
26. J. Hwang, L. A. Gheber, L. Margolis, M. Edidin, Domains in Cell Plasma Membranes Investigated by Near-Field Scanning Optical Microscopy. *Biophysical Journal* **74**, 2184-2190 (1998).
27. A. Branco, D. Francisco, T. Hanscheid, Is There a 'Normal' Oxygen Concentration for in vitro Plasmodium Cultures? *Trends Parasitol* **34**, 811-812 (2018).
28. A. D. Pillai *et al.*, Solute restriction reveals an essential role for clag3-associated channels in malaria parasite nutrient acquisition. *Mol Pharmacol* **82**, 1104-1114 (2012).
29. S. A. Desai, Insights gained from *P. falciparum* cultivation in modified media. *ScientificWorldJournal* **2013**, 363505 (2013).
30. H. Kim, U. Certa, H. Döbeli, P. Jakob, W. G. J. Hol, Crystal Structure of Fructose-1,6-bisphosphate Aldolase from the Human Malaria Parasite *Plasmodium falciparum*. *Biochemistry* **37**, 4388-4396 (1998).
31. M. A. Robien *et al.*, Crystal structure of glyceraldehyde-3-phosphate dehydrogenase from *Plasmodium falciparum* at 2.25 Å resolution reveals intriguing extra electron density in the active site. *Proteins: Structure, Function, and Bioinformatics* **62**, 570-577 (2006).
32. I. Pal-Bhowmick *et al.*, Cloning, over-expression, purification and characterization of *Plasmodium falciparum* enolase. *European Journal of Biochemistry* **271**, 4845-4854 (2004).
33. C. D. Smith, D. Chattopadhyay, B. Pal, Crystal structure of *Plasmodium falciparum* phosphoglycerate kinase: Evidence for anion binding in the basic patch. *Biochemical and Biophysical Research Communications* **412**, 203-206 (2011).
34. A. Patel *et al.*, ATP as a biological hydrotrope. *Science* **356**, 753-756 (2017).
35. D. T. McSwiggen, M. Mir, X. Darzacq, R. Tjian, Evaluating phase separation in live cells: diagnosis, caveats, and functional consequences. *Genes Dev* **33**, 1619-1634 (2019).
36. Y. Zhu *et al.*, The long noncoding RNA glycoLINC assembles a lower glycolytic metabolon to promote glycolysis. *Molecular Cell* **82**, 542-554.e546 (2022).
37. G. G. Fuller *et al.*, RNA promotes phase separation of glycolysis enzymes into yeast G bodies in hypoxia. *Elife* **9** (2020).
38. O. Yu, K. Masataka, Multipoint fluorescence correlation spectroscopy with total internal reflection fluorescence microscope. *Journal of Biomedical Optics* **14**, 014030 (2009).
39. T. Q. Binh *et al.*, Glucose metabolism in severe malaria: Minimal model analysis of the intravenous glucose tolerance test incorporating a stable glucose label. *Metabolism* **46**, 1435-1440 (1997).
40. D. Walliker *et al.*, Genetic analysis of the human malaria parasite *Plasmodium falciparum*. *Science* **236**, 1661-1666 (1987).
41. D. T. Riglar *et al.*, Super-resolution dissection of coordinated events during malaria parasite invasion of the human erythrocyte. *Cell Host Microbe* **9**, 9-20 (2011).
42. M. Morita *et al.*, PV1, a novel *Plasmodium falciparum* merozoite dense granule protein, interacts with exported protein in infected erythrocytes. *Sci Rep* **8**, 3696 (2018).
43. K. Motohashi, A simple and efficient seamless DNA cloning method using SLiCE from *Escherichia coli* laboratory strains and its application to SLiP site-directed mutagenesis. *BMC Biotechnology* **15**, 47 (2015).
44. M. J. van den Hoff, A. F. Moorman, W. H. Lamers, Electroporation in 'intracellular' buffer increases cell survival. *Nucleic Acids Res* **20**, 2902 (1992).

45. J. Schindelin *et al.*, Fiji: an open-source platform for biological-image analysis. *Nat Methods* **9**, 676-682 (2012).
46. Y. Kanda, Investigation of the freely available easy-to-use software 'EZR' for medical statistics. *Bone Marrow Transplant* **48**, 452-458 (2013).

Figures and Tables

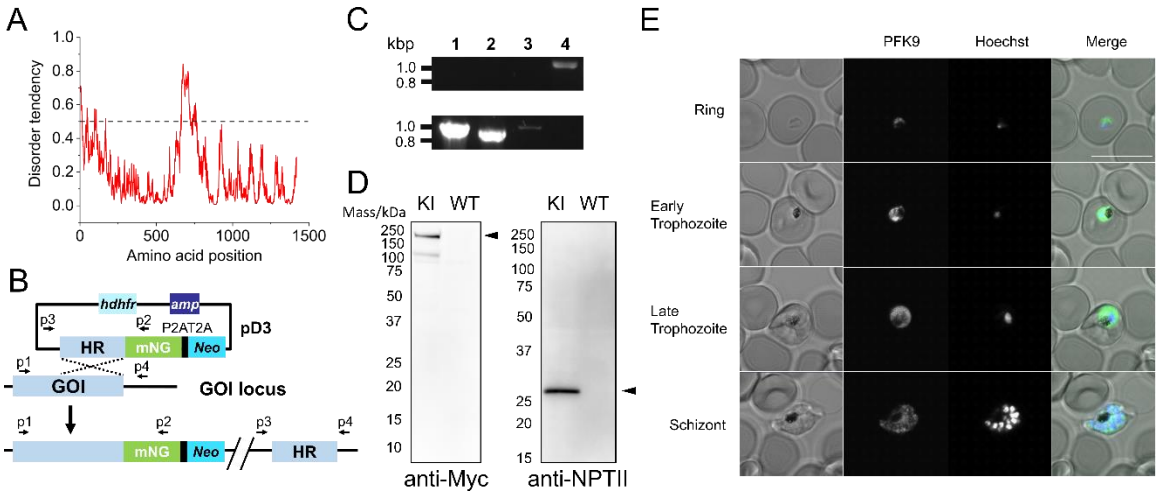

Figure 1. Generation of the *Pf*PFK9-mNG parasite. (A) The result of IUpred2A disorder prediction of *Pf*PFK9 suggesting the existence of *N*-terminal and *C*-terminal disordered regions. (B) Schematic of pKIC-ter plasmid and SLI. The plasmid has a homologous region of a gene of interest, following mNG, tandem skip peptides P2A-T2A, and NPT II, which shows G418 resistance only when inserted into the parasite genome. The skip peptides induce ribosomal skipping during translation, which allows separate expression of mNG-tagged GOI and neo proteins. (C) The results of diagnostic PCR for wild type (WT) and knock-in (KI) strains with different primer sets. Lane 1: p1 + p2, Lane 2: p3 + p4, Lane 3: p2 + p3, Lane 4: p1 + p4. (D) *C*-Terminal tagging of PFK9 in the *Pf* 3D7 parasite was confirmed by anti-Myc and anti-NPTII western blotting. Application of 2.5×10^7 parasite lysate/lane was used for WT and KI strains. The PFK9-Myc-mNG 190 kDa band and NPTII 29.1 kDa band were only observed in the KI samples, showing successful *C*-terminal tagging of PFK9. (E) Live imaging of the *Pf*PFK9-mNG parasite. PFK9 was uniformly expressed in the cytoplasm of the parasite throughout the asexual blood stage. G-body-like structures were not observed in the steady state. The scale bar represents 10 µm.

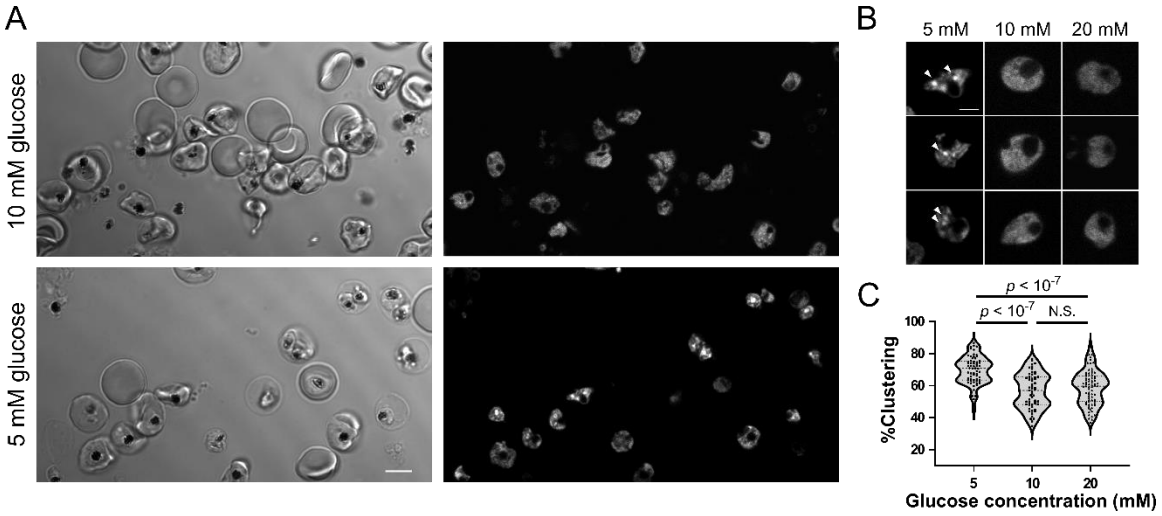

Figure 2. G-body-like structures formed in the *Pf*PFK9-mNG parasite under low glucose conditions. (A) Live imaging of the *Pf*PFK9-mNG parasite in a culture medium containing glucose at the indicated concentrations. The scale bar represents 5 µm. (B) A magnified version of the *Pf*PFK9-mNG parasite cultured in different glucose conditions. The arrowheads indicate the G-body-like PFK9 clusters observed in the 5 mM glucose culture. The scale bar represents 2 µm. (C) Clustering % of PFK9-mNG fluorescence in different glucose concentrations indicated the clustering of PFK9 occurred in a glucose concentration-dependent manner. n = 67 (5 mM), 53 (10 mM), and 59 (20 mM). p values were calculated by Kruskal–Wallis and Steel–Dwass post hoc tests.

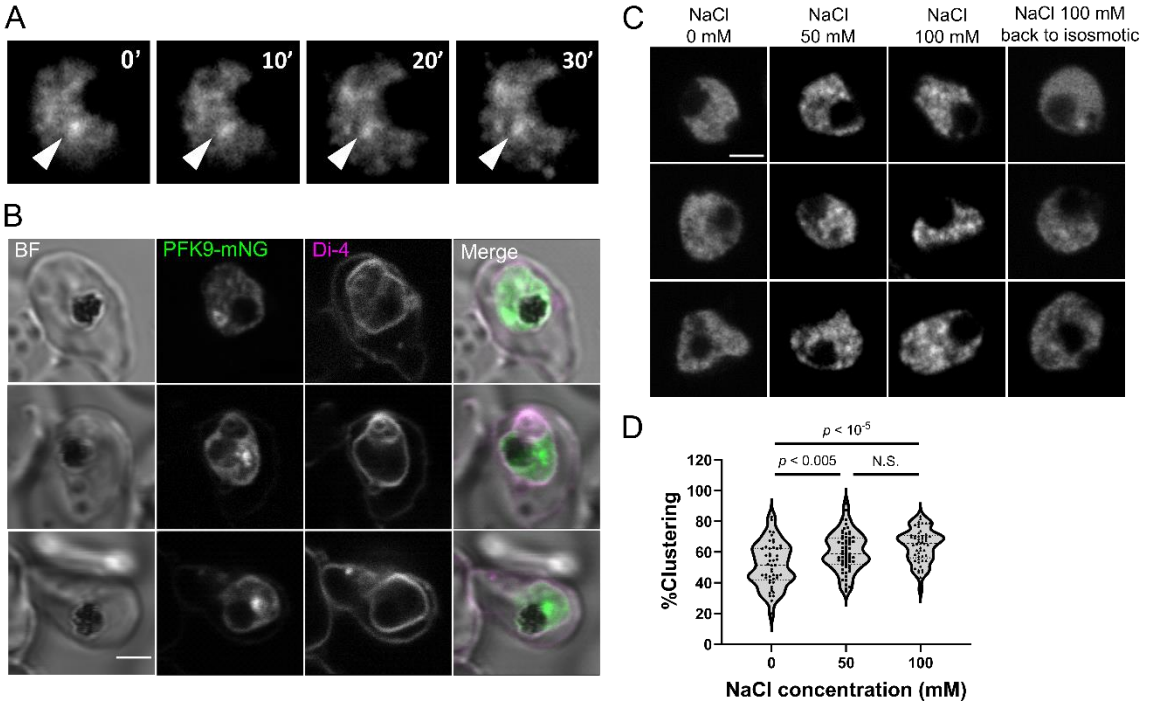

Figure 3. LLPS-like behavior of PFK9 clusters. (A) Time-lapse images of the *Pf*PFK9-mNG parasite over 30 min. The arrowheads indicate a representative stable G-body-like PFK9 cluster. (B) The *Pf*PFK9-mNG parasite was cultured in a low glucose medium and stained with the membrane probe Di-4-ANEPPDHQ for 30 min. The parasite plasma membrane and some inner membranes showed fluorescence, whereas the G-body-like PFK9 clusters were not stained with the dye. The scale bar represents 2 µm. (C) Live imaging of *Pf*PFK9-mNG parasites suspended in CM with the addition of the indicated NaCl concentration. PFK9 clusters were observed in the parasite cytosol and disappeared when the CM was reverted to isosmotic conditions. The scale bar represents 2 µm. (D) Clustering % of the *Pf*PFK9-mNG parasite indicated the clustering of PFK9 under osmotic stress. n = 48 (0 mM), 63 (50 mM), and 53 (100 mM). p values were calculated by Kruskal–Wallis and Steel–Dwass post hoc tests.

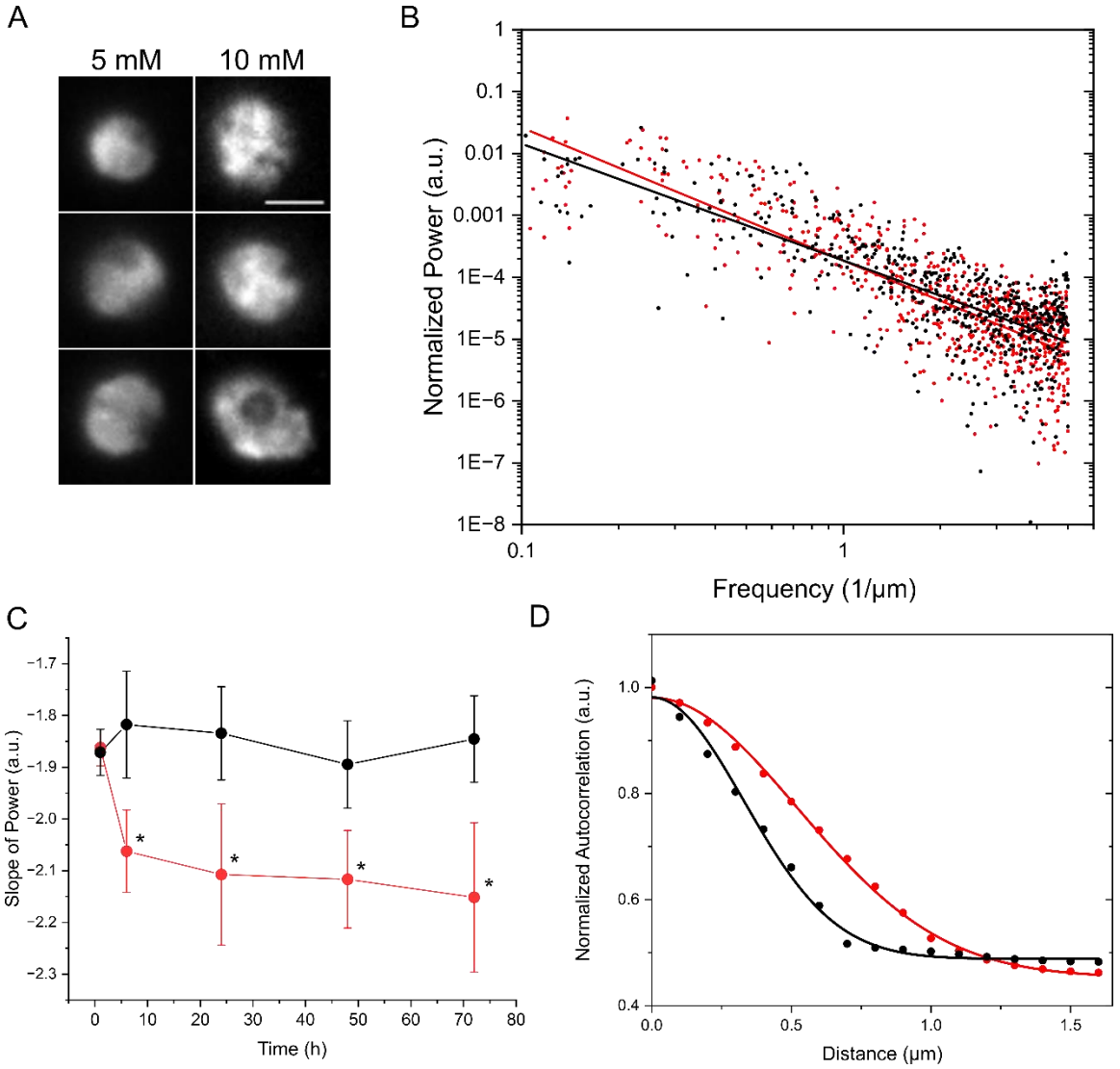

Figure 4. TIRF image analysis suggested the existence of larger PFK9 clusters in low glucose conditions. (A) Representative TIRF images of the *Pf*PFK9-mNG parasite cultured in 10 or 5 mM glucose-containing medium for 72 h. Tagged PFK9 was distributed non-homogeneously in the TIRF images. The scale bar represents 2 μm. (B) Double logarithmic plots of power spectra from line plots of the *Pf*PFK9-mNG parasite cultured in 10 mM (black) and 5 mM (red) glucose-containing medium for 72 h. The graph shows cumulative data from three different experiments, which analyzed six cells each and with more than three line plots per cell. (C) The slope values of power spectra regression lines from three different experiments suggested the existence of larger PFK9 clusters after 6 h of low glucose culture. The p-value was calculated using the Student's t-test. Error bars represent the standard deviation of the mean. *$p < 0.05$. (D) 2D-autocorrelation analysis of representative PFK9 fluorescence of the parasite cultured in 10 (black) and 5 (red) mM glucose-containing medium for 72 h also suggested larger PFK9 clusters occurred in low glucose conditions.

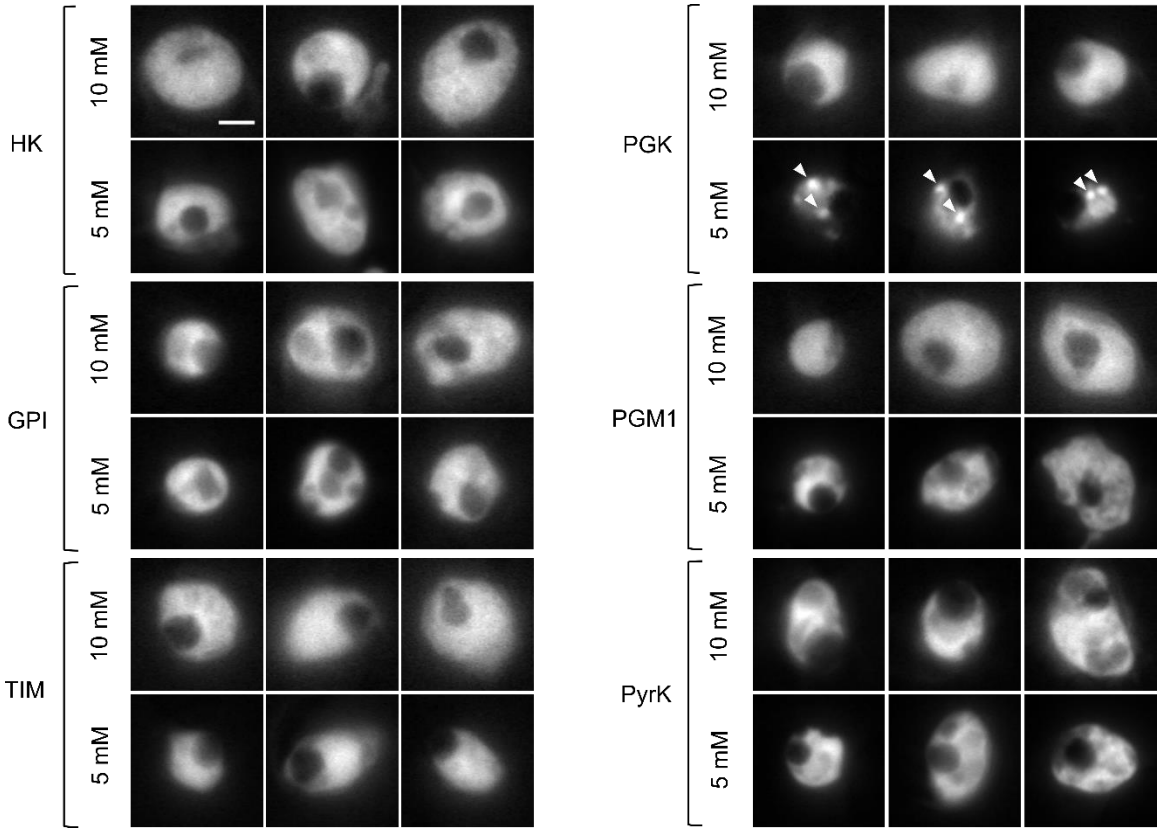

Figure 5. PGK also formed G-body-like clusters under low glucose conditions. Representative live images of the parasites that expressed tagged glycolytic enzymes cultured in different glucose concentrations for 80 h. Only PGK formed clusters in 5 mM glucose culture, as indicated by the arrowheads. The scale bar represents 2 µm.

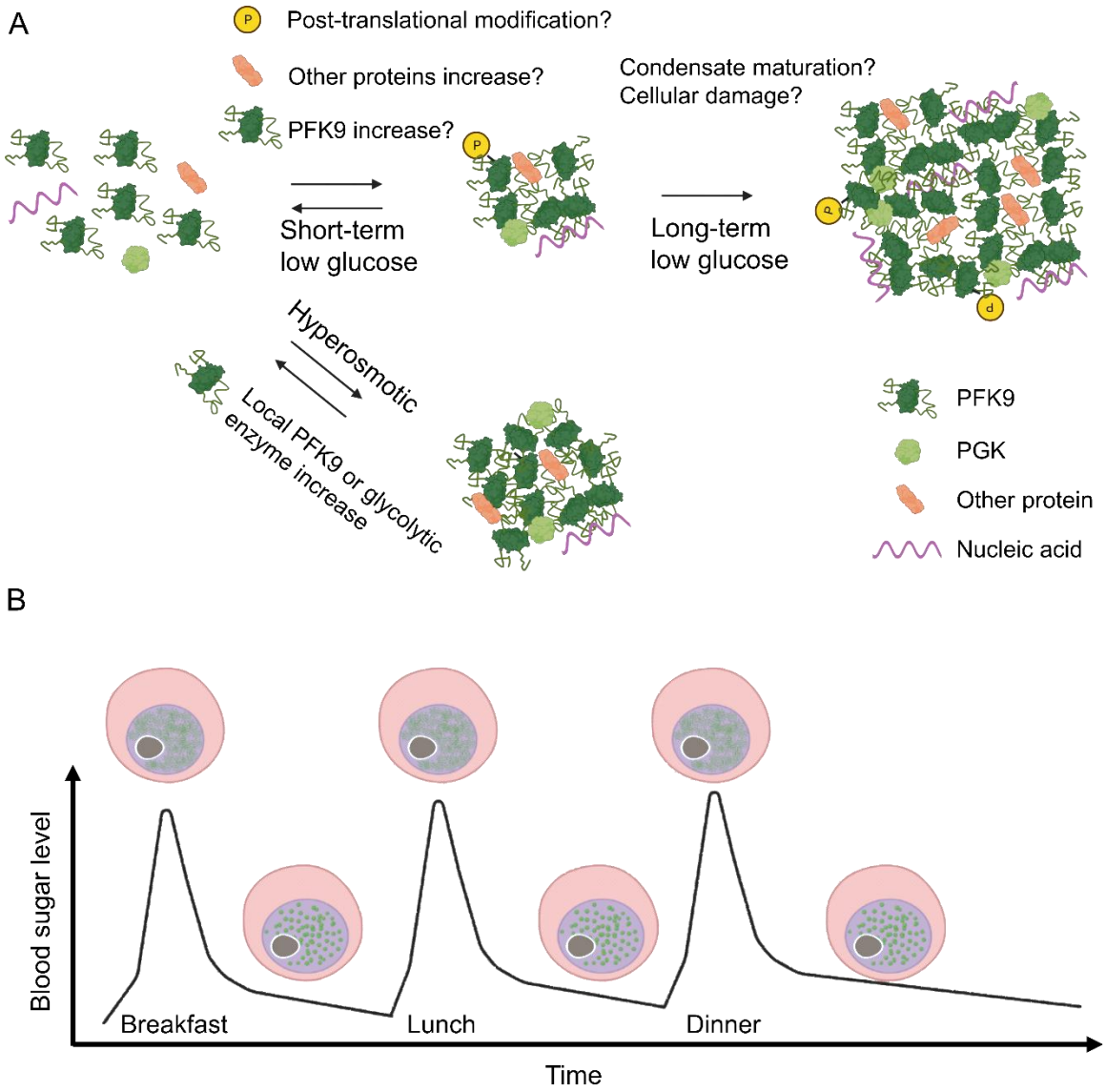

Figure 6. Possible models for G-body-like structure formation. (A) Reversible small G-body-like structures are formed after short-term low glucose culture and mature into irreversible large structures after long-term culture. The triggers for this clustering need to be elucidated. Hyperosmotic stress results in the formation of reversible medium sized G-body-like structures, possibly because of a rapid increase of the local PFK9 concentration. (B) Schematic of the formation of G-body-like structures along with oscillations in human blood sugar levels. The parasite may alter the glycolytic activity by the formation of these structures to adapt to different environmental conditions. Stage transition is not shown in this diagram.

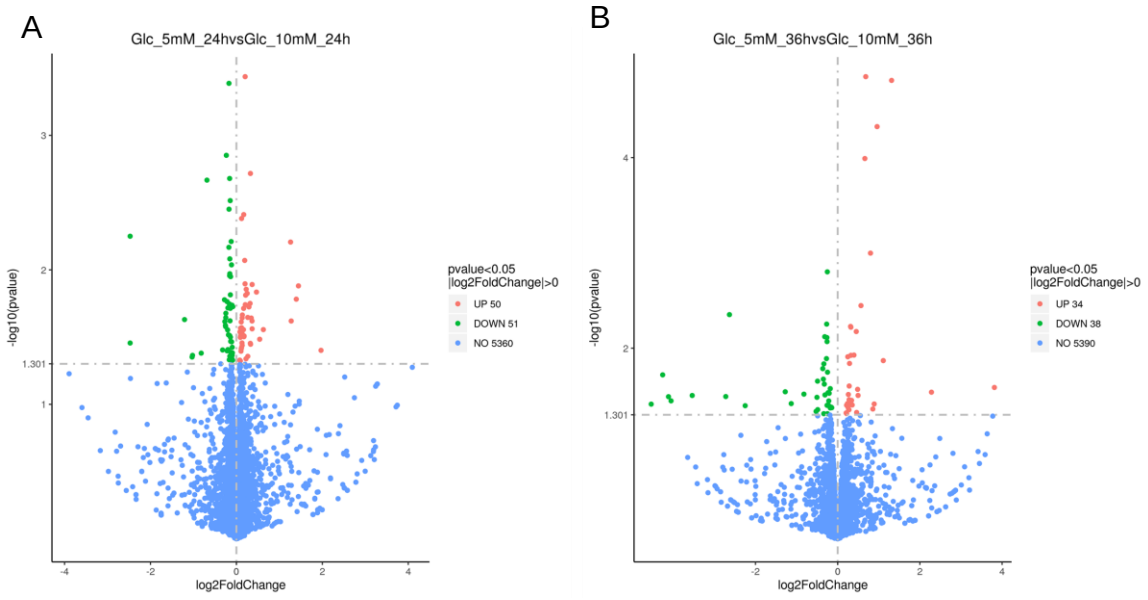

Figure S1. Transcriptome analysis of the parasite cultured in different glucose concentrations. Volcano plot showing differential expression of the parasite genes between 5 mM glucose and 10 mM glucose culture conditions at 24 (A) and 36 (B) h.

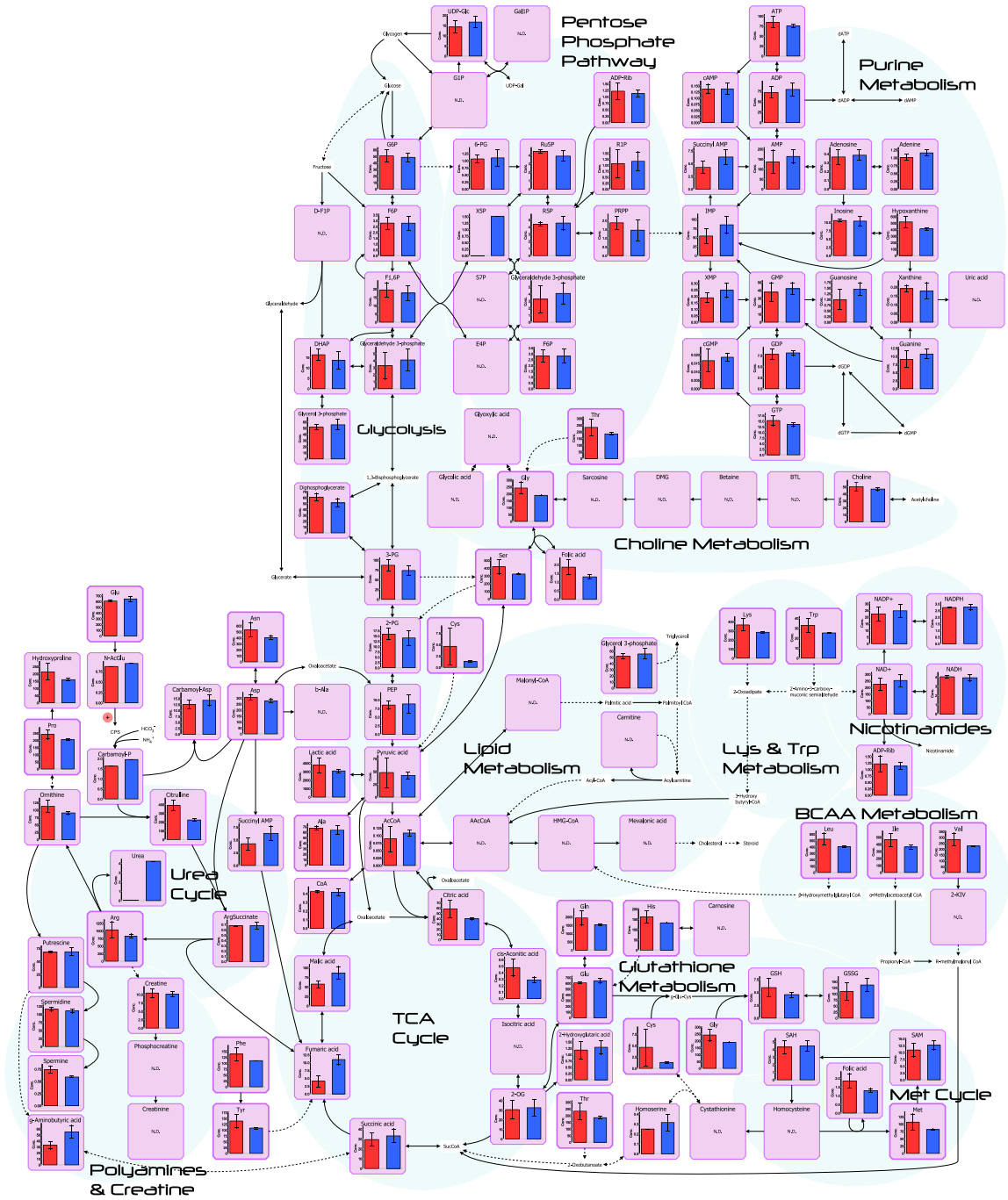

Figure S2. Long-term low glucose culture did not change the metabolic profiles of the parasite. The PFK9-mNG expressing parasite was cultured in 5 (red) or 10 (blue) mM glucose for 78–80 h, and 116 metabolites were measured in triplicate.

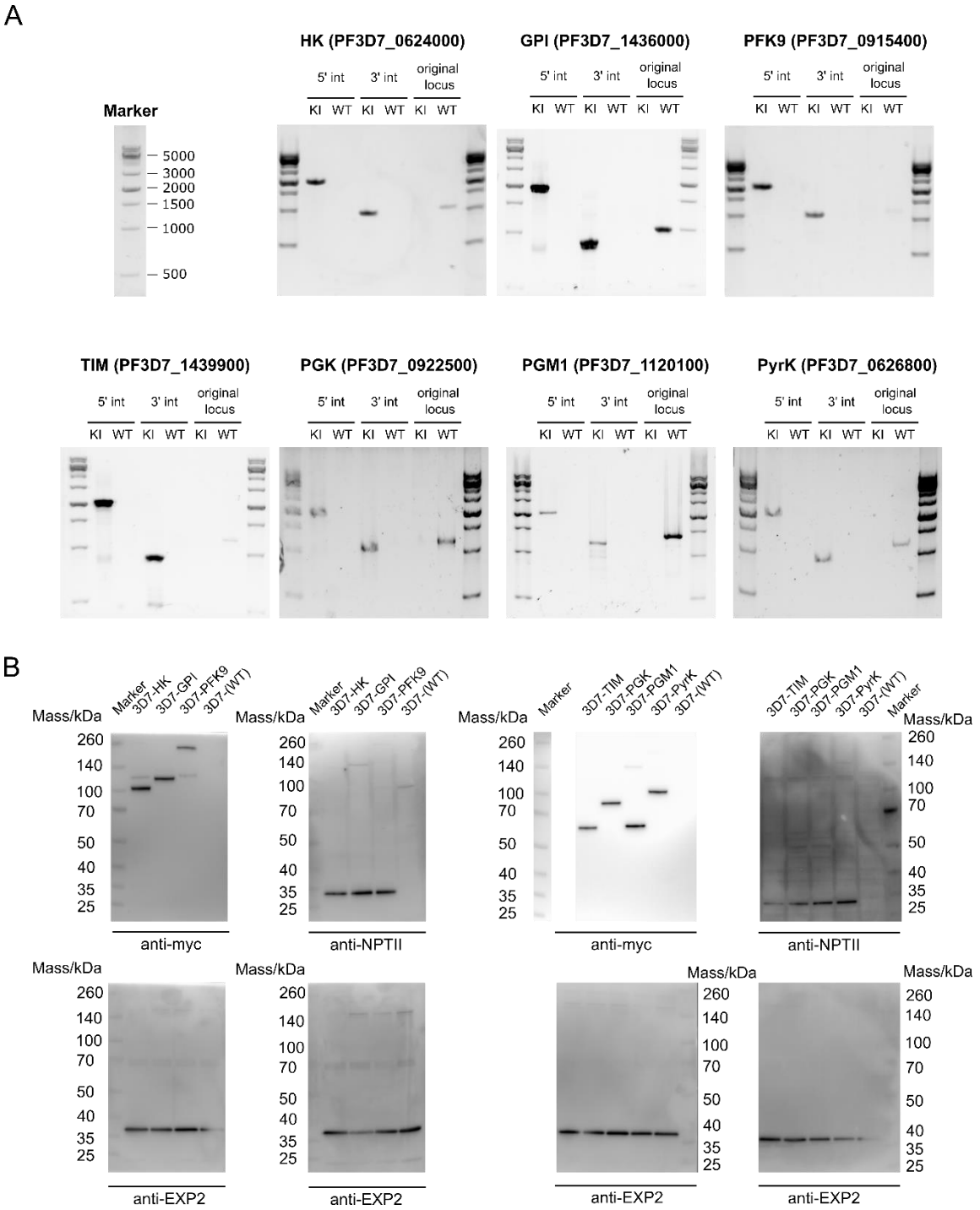

Figure S3. Generation of parasites expressing tagged glycolytic enzymes. (A) The results of diagnostic PCR for wild type (WT) and knock-in (KI) strains with different primer sets. (B) *C*-Terminal tagging of glycolytic enzymes in the *Pf* 3D7 parasite was confirmed by anti-Myc and anti-NPTII western blotting. Application of 5 × 10^6 parasite lysate/lane was applied. Estimated protein size: HK-mNG-my, 89.4 kDa; GPI-mNG-myc,101.5 kDa; PFK9-mNG-myc,193.6 kDa; TIM-mNG-myc, 62.0 kDa; PGK-mNG-myc, 79.5 kDa; PGM1-mNG-myc, 62.9 kDa; PyrK-mNG-myc, 89.8 kDa; NPTII, 29 kDa; and EXP2, 33.4 kDa.

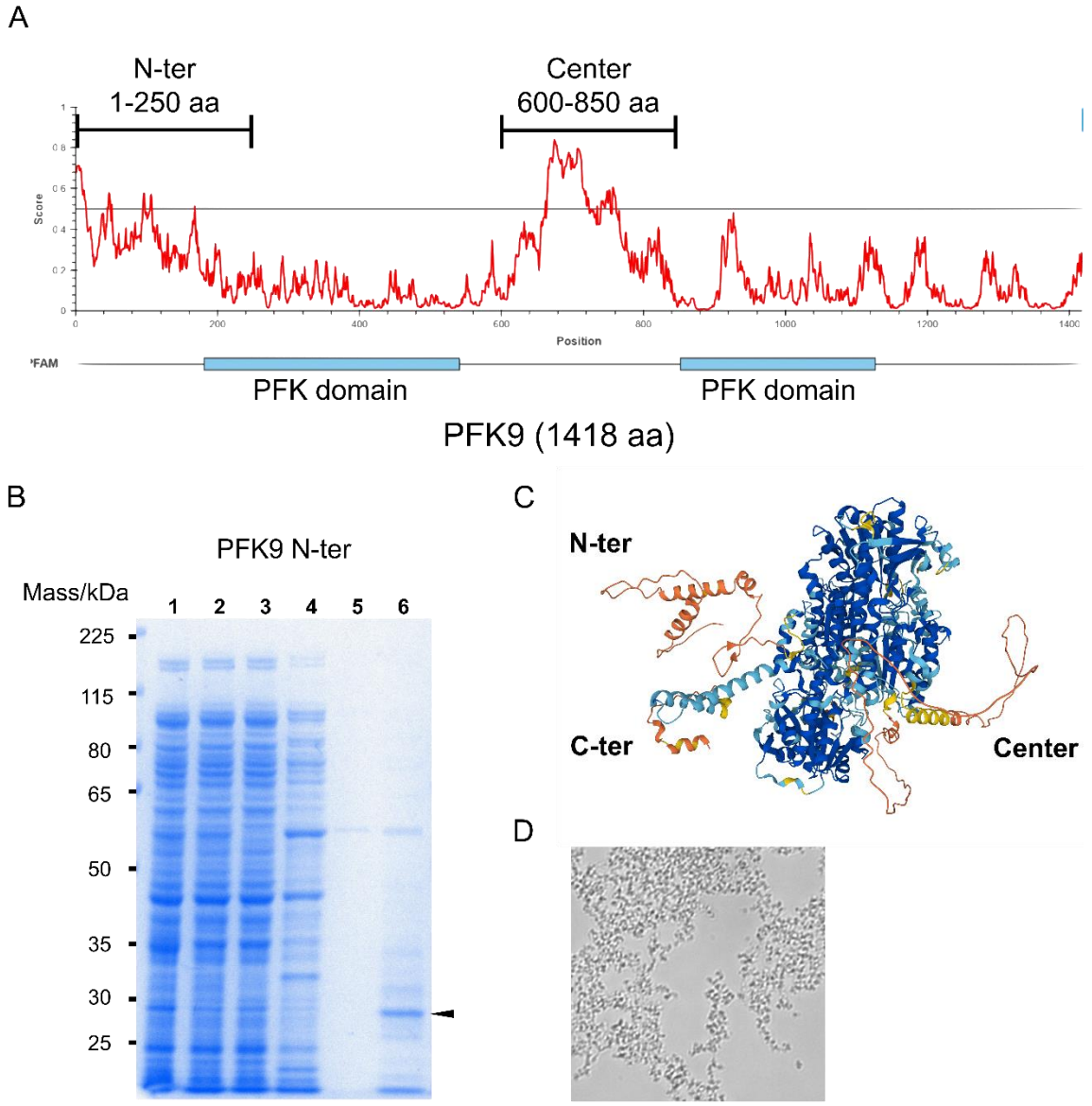

Figure S4. Purification of PFK9 intrinsically disordered regions. (A) The result of PFK9 disordered region prediction with IUPred2A and designs of PFK *N*-terminal (*N*-ter) and PFK9 center proteins. (B) The results of SDS-PAGE for PFK9 *N-ter* purification. The arrowheads show the purified target proteins. Lane 1: cell lysate, Lane 2: cytosol, Lane 3: flow through, Lane 4: wash with imidazole-containing buffer, Lane 5: wash with cleavage buffer, Lane 6: purified protein after cleavage. (C) Alphafold2 structure prediction of PFK9. (D) Representative brightfield picture of purified PFK9 *N*-ter protein aggregates.

Table 1. Analytical results of autocorrelation analysis.
The autocorrelation function of representative PFK9 fluorescence showed a good fit to a single Gaussian curve, and the estimated cluster size of low-glucose-cultured parasites was larger than that for the parasites cultured in normal glucose conditions. *The fitting errors were smaller than the pixel size of 100 nm.

Glucose concentration	Cluster size (nm)	R^2
10 mM	773 ± 100*	0.993
5 mM	1226 ± 100*	0.998

Table S1. Synthesized DNA sequences used for plasmid construction.

Name	Sequence
PfPGK	ACGTAACAGACTTAGGAGGGACCACTACTAGCCATTTTAGGTGGTGCTAAAGTATCAGATAAA ATTCAGTTAATCAAAAATTTATTAGATAAAGTTGATCGTATGATTATTGGAGGTGGTATGGCTTA TACTTTTAAAAAAGTCTTAAACAATATGAAAATTGGTACCTCTCTTTTTGATGAAGCAGGTAGTA AAATTGTTGGAGAAATTATGGAAAAGGCAAAAGCTAAAAATGTTCAAATATTTTTACCTGTAGAT TTTAAAATTGCAGATAATTTTGATAATAATGCTAATACCAAATTCGTTACTGATGAAGAAGGTAT CCCAGATAATTGGATGGGTCTTGATGCTGGTCCAAAAAGTATTGAAAATTATAAAGATGTTATT TTAACATCAAAAACTGTTATTTGGAACGGACCACAAGGTGTTTTCGAAATGCCAAACTTTGCAA AAGGTAGTATCGAATGTCTCAATTTAGTTGTTGAAGTTACCAAAAAAGGAGCTATCACCATTGT TGGAGGTGGAGATACAGCTTCATTAGTTGAACAACAAAATAAGAAAAACGAAATTAGTCATGTA TCTACAGGTGGAGGAGCCTCACTTGAACTTTTAGAAGGAAAAGAATTACCAGGTGTATTAGCA CTTTCAAACAAAATGGTGAGTAAGGGAGAAG
PfTIM	ACGTAACAGACTTAGGAGGTAGGACGTTGTTGTTTTTCCTGTTTCCGTACATTATGATCATACA AGGAAATTACTTCAGAGTAAGTTTTCTACTGGTATTCAGAATGTATCAAAATTCGGAAATGGAT CATACACAGGTGAAGTAAGTGCAGAAATTGCCAAGGATTTAAATATTGAATATGTTATTATTGG TCATTTTGAAAGAAGAAAATATTTCCATGAAACCGATGAAGATGTTCGTGAAAAATTACAAGCT TCATTAAAAAATAATTTAAAAGCCGTTGTATGTTTTGGTGAATCTTTAGAACAAAGAGAACAAAA TAAAACTATCGAAGTTATTACAAAACAAGTTAAAGCATTTGTTGATTTAATTGATAATTTTGATAA TGTTATTTTGGCTTATGAACCTTTATGGGCTATTGGTACTGGTAAAACAGCTACACCTGAACAA GCTCAATTAGTACACAAAGAAATCAGAAAAATTGTAAAAGATACATGCGGAGAAAAACAAGCTA ACCAAATAAGAATATTATATGGAGGTAGTGTTAATACTGAAAACTGCTCTTCATTAATTCAACAA GAAGATATTGATGGTTTCTTAGTTGGAAATGCTTCCTTAAAAGAATCTTTTGTTGATATAATAAA AAGTGCTATGATGGTGAGTAAGGGAGAAG
PfGPI	ACGTAACAGACTTAGGAGGTAGCAAAATTTATTAAAATTTTCAGCACATATTCAACAATTATCTA TGGAAAGTAATGGAAAATCAGTAGATAGAAATAATCAACCAATCCATTATAATACTTGTCAAGT ATATTTTGGTGAACCTGGTACAAATGGTCAGCATAGTTTTTATCAATTAATACATCAAGGACAA GTTATACCTGTTGAATTAATTGGATTTAAACATTCTCATTTCCCAATTAAATTTGATAAAGAAGTA GTAAGTAATCATGATGAATTAATGACTAACTTTTTTGCACAAGCTGATGCATTAGCTATTGGGA AAACATACGAACAAGTAAAAGAAGAAAATGAAAAAAATAAAATGTCTCCAGAATTATTAACTCAT AAAGTTTTTAACGGTAATAGACCATCAACCTTATTATTATTTGATGAATTAAATTTCTATACATGT GGTTTATTATTATCCTTATATGAAAGTAGAATTGTCGCTGAAGGATTTCTATTAAATATTAACAG CTTTGATCAATGGGGGGTAGAGTTGGGTAAGGTTCTAGCAAAAGAAGTAAGAAATTATTTTAAT GACACAAGAAATCAAAAGAAATCAGATAATACCTATAATTTTAATGAATCTACAAAAATTTTATT AAATTATTACTTGTCCAAAATGGTGAGTAAGGGAGAAG
PfPyrK	ACGTAACAGACTTAGGAGGTAGCCTTCCATTTATAGATGCAATTTACAAGGTAAACCAATTATC ACTGCCACTCAAATGTTAGAATCCATGACCAAGAACCCAAGACCAACAAGAGCAGAAGTTACA GATGTAGCTAATGCTGTTTTAGATGGTACTGATTGTGTTATGCTTTCAGGAGAAACTGCAGGTG GTAAATTTCCAGTGGAAGCTGTTACCATTATGTCCAAAATCTGTTTAGAAGCAGAAGCATGCAT TGATTATAAATTATTATATCAATCATTAGTAAATGCAATTGAAACACCAATTAGTGTTCAAGAAG CTGTGGCTAGATCAGCTGTAGAAACAGCAGAATCTATTCAAGCTTCTTTAATTATAGCTTTAAC AGAAACAGGTTATACGGCTAGATTAATTGCCAAATATAAACCAAGTTGTACCATCTTAGCCCTT AGTGCTTCTGATTCAACTGTTAAATGTTTGAACGTACACAGAGGTGTTACATGCATTAAAGTAG GTTCATTCCAAGGAACAGATATTGTTATTAGAAATGCTATTGAAATCGCAAAACAAAGAAATAT GGCAAAAGTTGGTGATAGCGTTATTGCTATTCACGGAATTAAAGAAGAAGTATCTGGAGGTAC CAACTTAATGAAAGTTGTACAAATTGAAATGGTGAGTAAGGGAGAAG

Table S2. Primers used for plasmid construction and diagnostic PCR.

Primer name	Sequence
PFK9_F1	acgtaacagacttaggaggGAGTTTAGCATTATTAAAGAC
PFK9_R1	taattcccggggtgttcatGTTCATTCTTTTTCTCTGGTT
HK_F1	ACGTAACAGACTTAGGAGGGTGCATATCAAAAAGGTAGAGGTAC
HK_R1	TAATTCCCGGGGTGTTCATTGGTAATTGTGGAATGTCC
PGM1_F2	acgtaacagactTAGgaggAGAATTTCAAATTCGACGTTG
PGM1_R2	CTTCTCCCTTACTCACCATTTTTGCTTTTCCTTGGTTG
p2	CGGTACCTTGACCTACCATATC
p3	caggaaacagctatgaccatg
PFK9_p1	GCTGATGTTGGAAAAAATTATG
PFK9_p4	GAAATATACACACATGGATAAATAC
HK_p1	TTCCCTTGTACATCACCTTCAAT
HK_p4	TCTTCACACACTCACATACAGACAA
PGM1_p1	GTGAAAGTACATGGAACAAGG
PGM1_p4	TATCCACAAATGGGAAACCTCG
PyrK_p1	ACCGCATCAGCTATTAGTTCC
PyrK_p4	ATACATTAAAGAAAGGCAAAGG
PGK_p1	TATTGAAGAAGAAGGTAAAGGTGTTG
PGK_p4	CATACATACACACATACAATAAG
TIM_p1	AGCAAACTGGAAATGTAATGGAAC
TIM_p4	ATATAGAATACGTTCACCTC
GPI_p1	TTTGGGATTGGGTAGGAGGTC
GPI_p4	AACCCATATTTGCACTTTCACAC

The lowercase letters indicate the sequences of the plasmid backbone

Table S3. Antibodies and reaction conditions used for western blotting.

Antibody name	Supplier	Dilution factor	Incubation time and temperature
Myc -Tag (9B11) Mouse mAb #2276	Cell Signaling Technology, Danvaese, MA, USA	500	1 hour, room temperature
Neomycin phosphotransferase II Antibody (4B4D1)	Novus Biologicals, Centennial, West Grove, CO, USA	500 or 1000	1 hour, room temperature
Anti-EXP2 Rabbit polyclonal antibody	Ehime University, Ehime, Japan	2500	1 hour, room temperature
Peroxidase AffiniPure Goat Anti-Mouse IgG (H+L)	Jackson ImmunoResearch, PA, USA	5000 or 10000	30 min, room temperature
Peroxidase AffiniPure Goat Anti-Rabbit IgG (H+L)	Jackson ImmunoResearch, USA	5000 or 10000	30 min, room temperature